cigre Turkey

TEPES
TURKISH JOURNAL OF ELECTRICAL POWER AND ENERGY SYSTEMS

DOI: 10.5152/tepes.2024.24021

RESEARCH ARTICLE

Axial Flux Permanent Magnet Motor Design for Lightweight Unmanned Aerial Vehicles

Faruk Kurtuluş[1], **Erdem Akboy**[1]

[1]Department of Electrical Engineering, Yildiz Technical University, İstanbul, Türkiye

Cite this article as: F. Kurtuluş and E. Akboy, "Axial flux permanent magnet motor design for lightweight unmanned aerial vehicles," *Turk J Electr Power Energy Syst.* Published online November 11, 2024. doi 10.5152/tepes.2024.24021

ABSTRACT

Axial flux permanent magnet (AFPM) motors are a type of electric motor in which the magnetic flux between the stator and rotor flows in the axial direction. These motors show superior performance compared to radial flux permanent magnet (RFPM) motors in industrial applications such as fans, industrial pump systems, and automotive industry, due to their ability to operate at high speeds, high-power density, and low flux path features. Nowadays, unmanned aerial vehicles (UAVs) are used in various fields such as mapping, firefighting, logistics, and military fields. High-efficiency, low-weight, and cost-effective motors have been gaining attraction for UAVs. In this paper, an AFPM is designed to achieve high-power density and efficiency in UAV applications. At the design stage, the essential flowchart and the equations used to calculate the dimensions of the AFPM motor are presented. Based on the presented equations, a three-phase axial flux motor simulation is carried out using the Ansys Electronics Desktop software, with a nominal power of 1 kW and a power density of 2.97 W/g, which can be used between 0-12500 rpm. The proposed design procedure is verified with the simulation results using finite element analysis.

Index Terms—Axial flux permanent magnet (AFPM) electric motor, finite elements analysis, unmanned aerial vehicle (UAV).

I. INTRODUCTION

Nowadays, due to the development of industry and technology, the usage areas of electric motors are increasing rapidly. This situation results in the necessity for electric motors to have smaller volumes and to operate with high efficiency. For this purpose, interest in permanent magnet (PM) electric motors instead of rotor-wound electric motors is increasing. PM electric motors are classified as radial or axial flux, depending on the direction of the magnetic field. Axial flux permanent magnet (AFPM) motors have magnetic flux that flows parallel with respect to the rotor and the motor's rotation axis, while in radial flux permanent magnet (RFPM) motors, the magnetic flux direction is radial and perpendicular to the rotation axis. AFPM motors outperform RFPM motors in applications due to their high-power density, short magnetic path, low cost, and volume [1-3].

AFPM motors are structurally classified as single stator single rotor (SSSR), double stator single rotor (DSSR), single stator double rotor (SSDR), and multiple stator multiple rotor according to the number of stators and rotors. Among these motor types, the SSSR AFPM motor gives the best results in terms of power density due to its simple structure with a single air gap [2].

The compact design of AFPM motors renders them particularly suited to applications such as electric vehicles (EVs), robots, and renewable energy systems. The design of AFPM motors is based on optimizing various parameters to improve the performance of the motor according to the application area. Design parameters such as magnetic positioning, stator winding structures, and cooling techniques are very important for increasing the efficiency and durability of the motor. Thus, optimizing these design parameters to achieve maximum efficiency and minimum loss is of great importance. For this purpose, many studies have been conducted in the literature to provide optimal design of AFPM motors for EV applications [4]. In addition, the correct selection of magnetic materials and PMs directly affects the performance of the motor. In the literature, the selection of PM materials with high-temperature resistance for motors is investigated, and factors such as magnetization, demagnetization, and temperature stability are considered [5,6]. In addition, the optimum design is aimed at different mathematical methods. In recent studies, yokeless and segmented armature AFPM topology has been studied, especially in EVs [7-9]. Studies comparing the performance of SSSR and SSDR motors designed in this topology are also available in the literature [10].

Received: July 31, 2024
Revision Requested: August 26, 2024
Last Revision Received: September 8, 2024
Accepted: September 29, 2024
Publication Date: November 11, 2024

Corresponding author: Faruk Kurtuluş, faruk.kurtulus@std.yildiz.edu.tr

The finite element analysis (FEA) is a method that produces approximate solutions to boundary value problems in general. It is widely used for modeling nonlinear and complex physical structures. Thus, FEA is an important numerically based and highly accurate method to analyze and simulate the nonlinear electromagnetic behavior of AFPM motors. There are studies on optimizing motor designs, estimating electromagnetic losses and the effect of rotor eccentricity on electromagnetic performance using FEA [11-14].

The utilization of unmanned aerial vehicles (UAVs) is now prevalent in a multitude of fields, including mapping, firefighting, logistics and military operations. The efficacy of these vehicles is contingent upon the effectiveness of the propulsion systems employed. In this context, in recent years, AFPM motors are often preferred in UAV applications where high-power density and compact design are required. Marcolini et al. [15] present a detailed analysis of an AFPM motor specifically designed and optimized for UAV propulsion. In this analysis, a multi-phase coreless and concentrated winding AFPM motor is designed to improve the performance of AFPM motors in UAV applications. The design phases, mathematical modeling, and results are analyzed in detail. In [16], the performance of SSDR AFPM motors for long-duration UAV applications is discussed. In this study, the output power, torque production, and efficiency of the motor are analyzed under different flight conditions, and the design criteria of suitable AFPM motors for long-duration missions are determined. However, the double air gap causes the motor dimensions to increase and makes the design difficult. In [17], the difficulties encountered during the integration of AFPM motors into miniaturized UAV platforms were examined. Important issues such as mechanical integration, electrical connections, and thermal management of the motors are addressed, and strategies are proposed for the successful integration of AFPM motors on UAV platforms. The effects of high energy efficiency of AFPM motors for swarming UAVs are investigated in [18]. In this context, the advantages obtained by optimizing energy efficiency are evaluated, and significant results are obtained on the potential of AFPM motors in swarming UAV applications. In [19], UAV applications in the literature are analyzed, and it is seen that AFPM motor technology is an important basis for next-generation UAVs.

A review of publications in the literature shows that AFPM electric motors have disadvantages such as manufacturing complexity and cost. There are studies examining the effects of stator geometry defects that occur in mass production processes on torque quality and knock torque [20]. To overcome these disadvantages, researchers continue to work on innovative manufacturing techniques and materials. There are also studies in the literature addressing recent developments to simplify manufacturing and reduce costs [21]. In the coming years, advances in materials science, integration with power electronics, and increasing interest in environmentally friendly manufacturing processes will increase the use of AFPM electric motors in UAVs [22].

There are a number of AFPM motor designs in the literature for different purposes [15, 23-25]. However, studies focusing on lightweight UAV applications are not very common. Nevertheless, a comparison of some AFPM motor designs made in the past and some key features of the AFPM motor design subject to this study is presented in Table I.

In this study, an SSSR AFPM motor with high-power density and efficiency is developed to serve as a reference for UAV applications. In this context, a three-phase AFPM motor with a nominal power of 1 kW and a power density of 2.97 W/g, which can be used in the range of 0–12500 rpm, is designed and simulated, and the design is validated with the simulation results using FEA. The design of the AFPM motor with the SSSR structure proposed in this study is realized by considering the design algorithm given in Fig. 1. The presented design algorithm requires the determination of constraints and initial electromagnetic design at the beginning. The initial design is first subjected to analytical and then numerical analysis. In these analyses, the torque characteristics of the machine are examined and optimization is made to improve the torque quality. Then, losses, demagnetization, saturation conditions, and other motor parameters are examined using FEA. After that, the electromagnetic design is finalized.

The sections of the paper are listed as follows: In the second section, the design studies are mentioned. Then the sizing equations used for the proposed AFPM motor are given and explained. The initial

Main Points

- In this paper, an axial flux permanent magnet electric motor is designed, and the design is subjected to analytical and then numerical analyses.
- The design is aimed to be used especially in lightweight unmanned aerial vehicles, and it is aimed to create an alternative approach for motors frequently used in these platforms.
- The design algorithm used during the design studies is given, and the theoretical information about the dimensional equations of an electric motor is presented to the readers.

TABLE I.
COMPARASION OF LATEST DESIGNS IN THE LITERATURE

	Design 1	Desing 2	Desing 3	Desing 4	Proposed Design	Unit
Rated speed	15 000	1285	1500	800	7500	rpm
Rated torque	0.7	17.1	6.3	120	2.67	Nm
Rated voltage	24	210	48	108	36	V
Output power	1000	2200	1000	10 000	2000	W
Topology	SSDR	SSSR	SSSR	SSDR	SSSR	–
Number of pole	10	28	4	20	20	–
Number of slot	12	24	30	60	18	–
Efficiency	94.5	≥80	90.5	93	91.5	%

SSDR: Single Stator Double Rotor; SSSR: Single Stator Single Rotor.

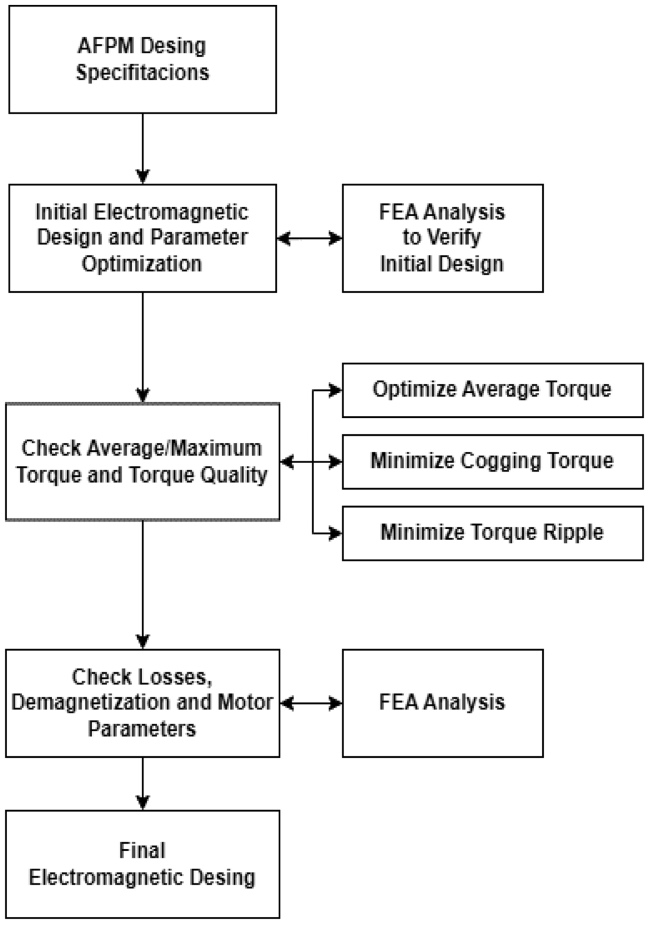

Fig. 1. Axial flux permanent magnet (AFPM) desing algorithm.

parameters of the design are presented, and the steps of designing the motor components using Ansys Electronics Desktop software are described. The design is solved analytically and verified by FEA. In the fourth section, the results of these analyses are presented in tables and graphs.

II. AFPM DESIGN STUDIES

The AFPM motor design using this design algorithm is analyzed with the RMxprt extension of the Ansys Electronics Desktop, and the obtained analytical solutions are verified by FEA using Maxwell 2D.

A. Dimensional Equations

The first stage of the design process is to estimate and determine the required dimensions of the motor, such as the outer diameter and active length of the machine. This estimation is necessary to meet the power and torque requirements within certain constraints, including inverter voltage and current limits, maximum geometric dimensions, and cooling conditions. In this context, using sizing equations is a traditional and widely accepted approach. In the rest of the paper, some sizing equations used in the literature are given.

General sizing and power density equations are used to compare various types of electrical machines [26]. These equations are developed by excluding stator leakage inductance and resistance. The following equation is used for the output power P_R of any electrical machine:

$$P_R = \eta \frac{m}{T} \int_0^T e(t) i(t) dt = \eta m K_p E_{pk} I_{pk} \quad (1)$$

In these equations, machine efficiency η, number of phases m, phase back electromotive force E_{pk}, and current peak values I_{pk} and K_p is the power factor. The equation for K_p is given below [26].

$$K_p = \frac{1}{T} \int_0^T \frac{e(t) i(t)}{E_{pk} I_{pk}} dt \quad (2)$$

K_p is determined by analyzing the back electro motor force and current waveform for a specific machine type. The values corresponding to K_p are summarized in [26] for various waveforms. Finally, the general-purpose sizing equation (3) for AFPM motors can be used as given in [27].

$$P_R = \frac{1}{1+K_\phi} \frac{m}{m_1} \frac{\pi}{2} K_e K_i K_p K_L \eta B_g A \frac{f}{p} \left(1-\lambda^2\right) \left(\frac{1+\lambda}{2}\right) D_o{}^3 \quad (3)$$

where, $K_\phi = A_r/A_s$ is the ratio of the electric loads on the rotor and stator, m_1 is the number of phases of the stator, K_e is the electromagnetic compatibility winding factor including the winding distribution factor and the ratio between the radiated field, K_i is the current waveform factor, B_g is the air gap flux density, $A = A_r + A_s$ is the total electric charge, f is the frequency, p is the number of pole pairs, $K_L = D_o/L_e$ is the ratio of the outer surface diameter to the effective length of the AFPM motor, and $\lambda = D_i/D_o$ is the ratio of the inner surface diameters to the outer surface diameters. For the TORUS-type AFPM motor, the average electromagnetic torque T_e can be expressed as given in the following equation, assuming a sinusoidal waveform for the air gap flux density and $K_e = \pi$.

$$T_e = \frac{\pi}{4} K_i K_p B_g A_s \left(1-\lambda^2\right) . \left(\frac{1+\lambda}{2}\right) . D_o^3 \quad (4)$$

The simplified electromagnetic torque equation (4) given above is used to optimize the diameter ratio to achieve maximum torque. Even if the optimization criterion remains consistent for a given set of electrical loads and flux densities, the optimum value may vary depending on different factors such as rated power, pole pairs, converter frequency, and machine structure.

To evaluate the power density of an AFPM motor, several basic parameters are taken into account, such as the axial lengths of the stator and rotor cores (L_{cs}, L_{cr}), the axial length of the PM, and the radial projection of the end winding from the iron stack (W_{cu}). These parameters depend on factors such as flux densities in different parts of the machine, electrical loading, current density, and slot filling factor.

The prediction equations may vary in the analysis for different types of AFPM motor designs. In such cases, either FEA-based or empirical correction factors are applied in the literature to adjust the prediction results. The accuracy of FEA-based methods is higher than empirical methods. The formulas used for the estimating equations are given as follows, respectively.

The stator core axial length L_{cs} is calculated as specified in reference [28], assuming W_{cu} is equal to the stator slot depth.

$$L_{cs} = \frac{B_g \pi \alpha_p D_O \left(1+\lambda\right)}{4pB_{cs}} \tag{5}$$

where B_{cs} is the stator-core flux density and α_p is the ratio of the average air-gap flux density to the peak air-gap flux density. With a similar assumption, the rotor core axial length (L_{cr}) is expressed as in [28].

$$L_{cr} = \frac{B_u \pi D_O \left(1+\lambda\right)}{8pB_{cr}} \tag{6}$$

where B_{cr} is the rotor-core flux density and B_u is the achievable flux density at the PM surface. For the toroidal winding, W_{cu} is estimated as in equation (7) and is equal to the stator slot depth in [28].

$$W_{cu} = \frac{D_i - \sqrt{D_i^2 - \frac{A\left(D_i + D_O\right)}{k_{cu} J_s}}}{2} \tag{7}$$

In this equation, k_{cu} is the copper fill factor, and J_s is the current density. The PM length L_{PM} for a TORUS-type AFPM motor is calculated as follows.

$$L_{PM} = \begin{cases} \dfrac{\mu_r B_g}{B_r - \dfrac{B_g K_f}{K_d}} \left(g + W_{cu}\right), \ slotless \\ \dfrac{\mu_r B_g}{B_r - \dfrac{B_g K_f}{K_d}} \left(K_c g\right) \ slotted \end{cases} \tag{8}$$

In these equations, μ_r is the relative permeability of the magnet, g is the air gap thickness, B_r is the residual flux density of the *PMs*, K_d is the leakage flux factor, K_c is the carter factor, and K_f is the corrected peak value factor of the air gap flux density in the radial direction.

In the sizing equations for AFPM motors, it is essential that the electric and magnetic loads, including flux densities, electric charges, current density, etc., on the various motor components are well defined. This definition is crucial to accurately estimate the primary geometric dimensions of the AFPM motor. The magnetic flux density and armature currents in different motor components depend on factors such as power rating, material properties, and motor geometry. To improve the accuracy of the sizing equations, the magnetic flux density in different motor components under no-load conditions is usually estimated using FEA. These estimated values are then used to optimize the parameters in the sizing equation.

B. Desing Parameters

For the design of the proposed SSSR AFPM motor, the values given in Table II are taken into consideration.

The values presented in the table are the values decided by the designers, and these values were chosen considering the scenario of using the designed AFPM motor in a fixed/rotating wing lightweight class UAV. Based on these parameters, rotor and stator designs and winding factors are calculated, and design results are given.

TABLE II.
INITIAL DESING PARAMETERS

Parameter	Value	Unit
Rated speed	5000	rpm
Maximum speed	12 500	rpm
Operating voltage	36	V
Nominal output power	1000	Watt
Efficiency	>90%	–
Cooling method	Air cooling	–
Number of phase	3	–
Number of pole	20	–
Number of slot	18	–

C. Rotor Design

In the proposed AFPM motor, the outer and inner diameter dimensions of the rotor are 100 mm and 60 mm, respectively, and the thickness is selected as 5 mm. In this motor with SSSR topology, magnets are placed on the rotor. When choosing a magnet, it is important to choose one that will provide the required magnetic field. Choosing a magnet with an unnecessarily large or small magnetic force reduces the design efficiency. One of the most important factors affecting the torque and efficiency values expected from the design is the relationship between the magnetic field created by the selected magnet and the magnetic field created by the current flowing through the windings. In this design, an NdFe52-type magnet was used. "Steel-1010" is selected as the rotor material. Thus, the cost of the motor design is reduced. The stacking factor of the rotor is 0.95, and the ANSYS interface view of the rotor is shown in Fig. 2.

D. Stator Design

When sizing the stator, the priority is to adjust the air gap between the stator and the rotor. When trying to minimize the air gap, production and handling processes are also considered. In addition, as a result of the analysis, the air gap between the stator and rotor was determined to be 0.75 mm. The area covered by the stator and the material from which the stator is manufactured are factors that affect the magnetic flux that the stator can store. The dimensions of the stator were chosen as 100 mm and 60 mm for the outer diameter and inner diameter, respectively, plus a stator core length of 25 mm and a stacking factor of 0.90. As mentioned before, the number of slots in the stator is set to 18. Thus, the designed stator geometry is shown in Fig. 3.

The dimensional and structural parameters of the designed motor are presented in Table III.

Different winding techniques can be used in brushless DC motors, as in most electric motors. In this design, the "Whole coiled – concentric winding" technique, which is one of the commonly used winding patterns shown in Fig. 4, is used. In order to make the design

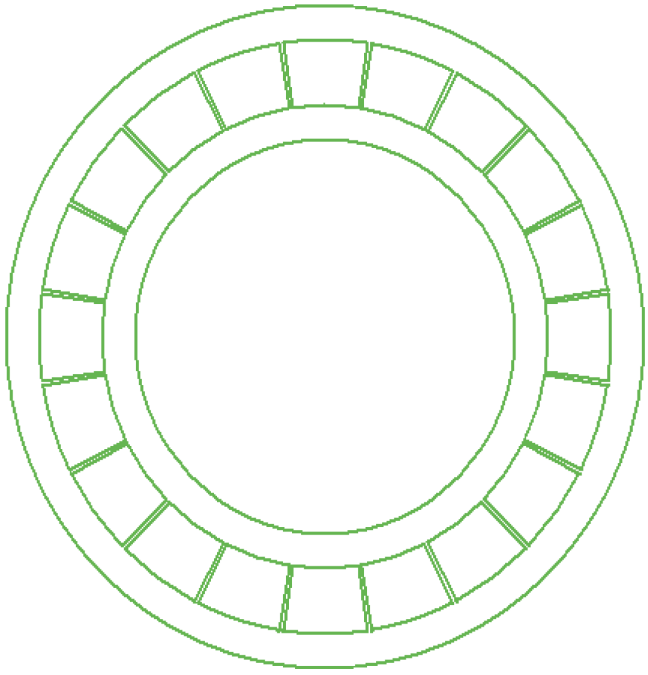

Fig. 2. Rotor design.

realizable, the slot fill ratio was chosen as 65%. However, it was observed that by increasing this ratio during the design, even better results were obtained in terms of efficiency.

Here, although the slot area is 104 mm^2, the net slot area is 102.83 mm^2. One of the factors affecting this is the thickness of the insulators to be used on the stator.

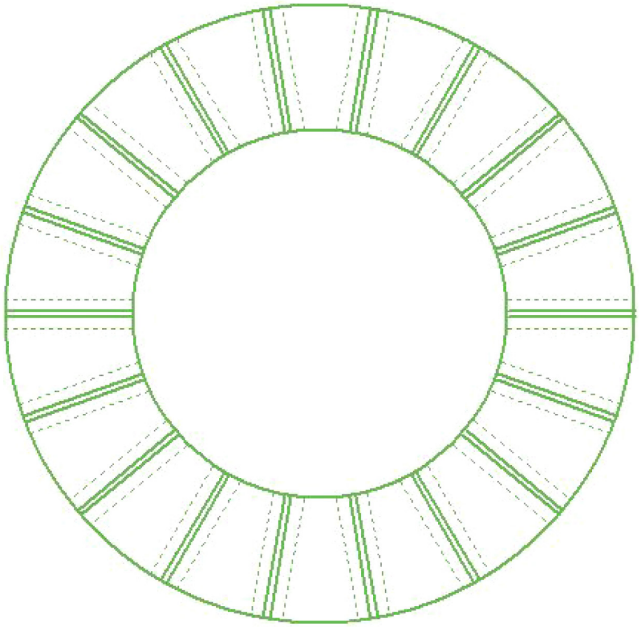

Fig. 3. Stator design.

TABLE III.
DIMENSIONAL PARAMETERS

Parameter	Value	Unit
Outer radius	100	mm
Inner radius	60	mm
Total axial length	32.75	mm
Magnet type	NdFe52	–
Magnet thickness	2	mm
Air gap	0.75	mm
Stacking factor of rotor	0.95	–
Stacking factor of stator	0.90	–

In half-molded windings, the entire slot is filled with one winding. This results in lower winding resistance but a higher inductance value. In full molded windings, two different phase windings are placed in one slot. This causes the winding resistance to be higher than that of the half-molded winding and the inductance value to be lower than that of the half-molded winding [29, 30].

As a result of the analysis, the number of parallel branches was decided to be 1. The number of conductors per slot was determined to be 4, and 34 wires were used per conductor. In order to make the design realizable, copper wire with a diameter of 0.5 mm was used, and the thickness of the insulator on the wire to be used was measured as 0.1 mm.

The winding factor is defined as the product of the distribution factor (K_d) and the coil clearance factor (K_c). This factor is important in terms of the effective value of the voltage produced in AC machines, the

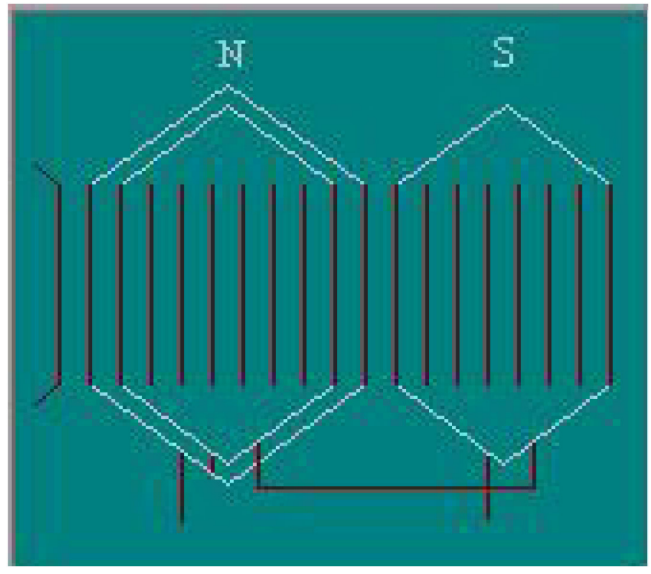

Fig. 4. Whole coiled winding.

torque, and the improvement of harmonics that cause a decrease in efficiency. The winding factor is a measure of whether the distribution of the winding on a rotor to the stator is homogeneous. It expresses how much the magnetic flux of a coil/winding acts on a peripheral area of diagonal unit length.

In this study, 18 slot and 20 pole combinations were selected according to the desired torque and speed values. The winding factor of this slot/pole combination was determined to be 0.94521. At the same time, this slot/magnet pole combination has 180 gear pitches per rotation.

The 3D design visuals of the motor, designed by considering the rotor and stator design parameters given above, are given in Fig. 5.

III. ANALYSIS RESULTS

In this proposed AFPM motor design process, simulation studies were carried out for a three-phase AFPM motor with a nominal power of 1 kW and a power density of 2.97 W/g, which can be used between 0–12 500 rpm. The RMxprt extension of the Ansys Electronics Desktop software was used for analytical solutions, and magnetic analysis was performed with the FEA in Ansys Maxwell 2D. In the analysis, it was aimed to examine the characteristics of the designed motor under a 1000 W constant load. In order to achieve this, the load type was defined as "constant power" in the RMxprt analytical solutions phase, and the amount of load was 1000 W.

A. Analytical Results

The results of the analysis show that the maximum efficiency of the motor is 91.51%, which is above the target value. The efficiency of the motor obtained as a result of the studies carried out at certain speed ranges is shown in Fig. 6.

Fig. 7 shows the power–rpm curve of the proposed motor. During the design, it is aimed to operate the motor at nominal 1 kW and a maximum 3 kW. Since this prototype motor to be produced is aimed to operate mostly around 5000–10,000 rpm, the desired design parameters are successfully achieved.

Since the motor is started to operate under a constant load when it is stationary, the torque response starts above 200 Nm as seen in the graph and goes through 0 at the end of the analysis. According to the results, the designed motor provides a torque of 2 Nm and above up to approximately 10,000 rpm. Fig. 8 shows the torque–rpm curve.

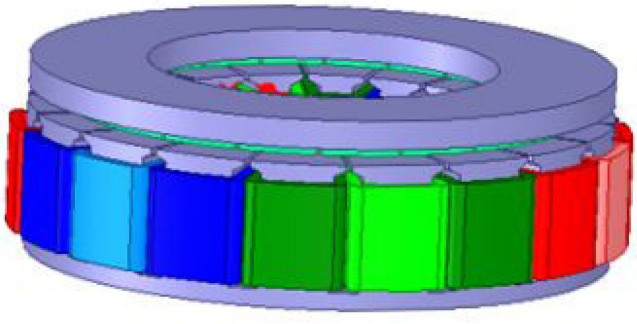

Fig. 5. 3D visual of the Axial flux permanent magnet (AFPM) motor design.

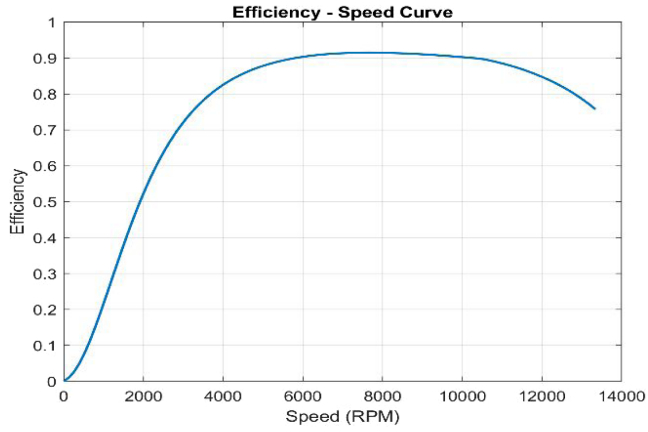

Fig. 6. Efficiency–speed curve.

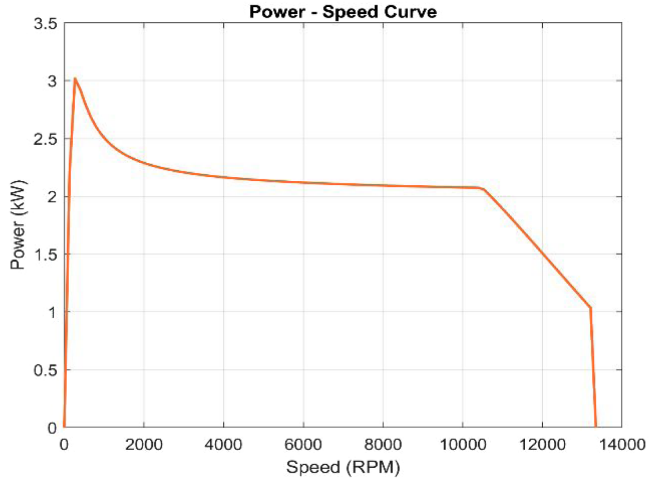

Fig. 7. Output power–speed curve.

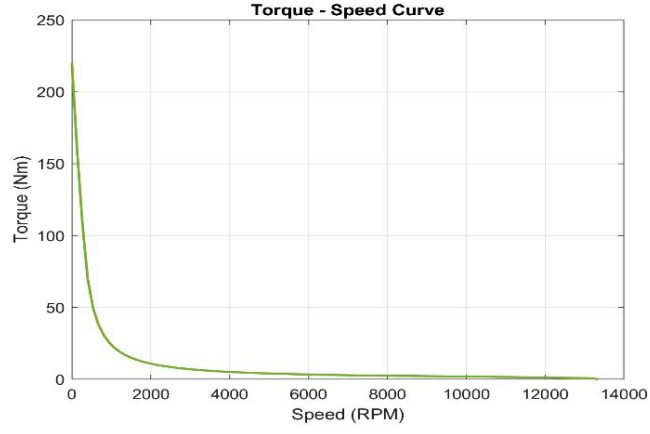

Fig. 8. Torque–speed curve.

TABLE IV.
RESULTS OF ANALYTICAL SOLUTION

Performance Parameter	Value	Unit
Average input current	36.69	A
Iron loss	308	W
Armature copper loss	3.99	W
Output power	2098	W
Efficiency	91.5	%
Speed	7496	rpm
Torque	2.67	Nm
Maximum output power	3001	W
Weight	1.01	kg
Power density	2.97	W/kg

The analysis was carried out under a constant load of 1000 W, a nominal voltage of 36 V, a temperature of 75 degrees Celsius, and a rated speed of 5000 rpm. The data obtained as a result of analytical solutions for the AFPM motor designed for UAV applications are presented in Table IV.

B. FEA Results

In the numerical analysis performed using FEA, Maxwell 2D was used. The value of 5000 rpm, determined as the nominal operating speed, was defined as speed information in Maxwell 2D and FEA was run at this point.

The magnetic field created by the current flowing through the windings should not be more than the material in the stator can store. This is very important for efficiency. In order to see the magnetic flux density across the stator, the design should be analyzed in ANSYS Maxwell. Fig. 9 shows the result of the analysis. It is clear from this figure that the stator material - magnetic flux relationship is quite adequate and appropriate according to the analysis result.

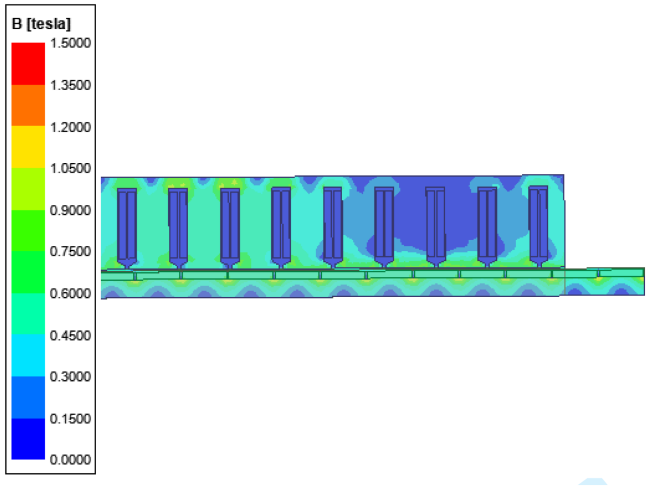

Fig. 9. Magnetic analysis in Maxwell 2D.

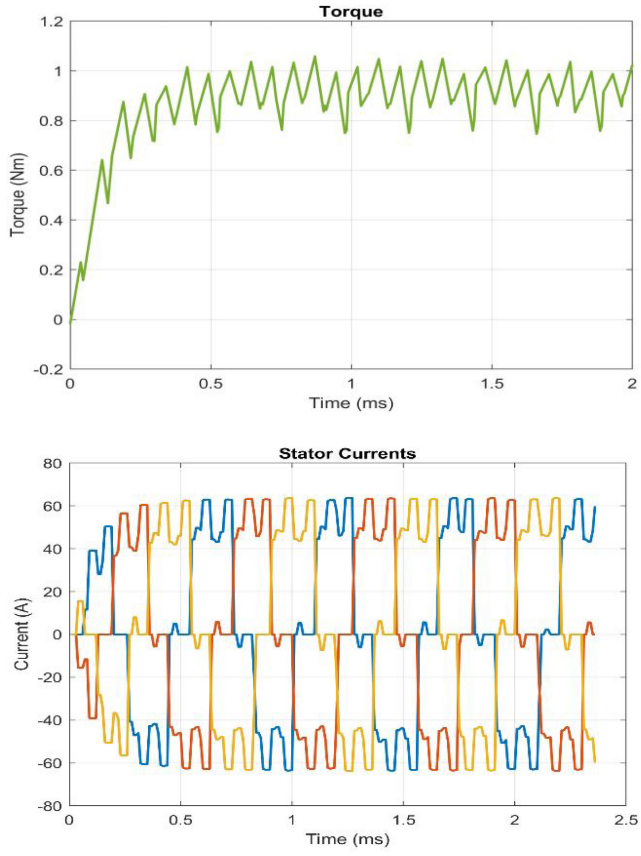

Fig. 10. FEA results for stator phase currents and output torque.

The total duration of the FEA performed using Maxwell 2D was determined to be 2 ms and the time step was determined to be 0.1 ms. In Fig. 10, the stator phase currents and motor output torque graphs obtained as a result of the FEA are presented together.

IV. CONCLUSION

Power density is an important factor for the vehicle's lift rate and hover time in UAV applications. In addition, AFPM motors exhibit higher performance in UAV applications than radial flux electric motors due to their advantages such as efficiency, cooling, high speed, etc. SSSR AFPM electric motors are widely preferred in applications due to their stable structure and applicability. In this study, a three-phase AFPM motor with a nominal power of 1 kW and a power density of 2.97 W/g, which can be used between 0–12 500 rpm, is proposed for light and medium class UAV applications. The design of the proposed electric motor is carried out using Ansys Electronics Desktop software, and FEA is used to validate the analysis. According to the analysis results, the proposed SSSR AFPM motor is suitable for UAV applications in terms of efficiency, size, power, and power density.

Availability of Data and Materials: The data that support the findings of this study are available on request from the corresponding author.

Peer-review: Externally peer-reviewed.

Author Contributions: Concept – F.K., E.A.; Design – F.K.; Supervision – E.A.; Resources – F.K., E.A.; Materials – F.K., E.A.; Data Collection and/or Processing – F.K.; Analysis and/or Interpretation – F.K.; Literature Search – F.K.; Writing – F.K.; Critical Review – E.A.

Declaration of Interests: The authors have no conflicts of interest to declare.

Funding: This study received no funding.

REFERENCES

1. M. Ebadpour, and M. R. A.Pahlavi, "Performance analysis and the cost effective position sensorless control of axial flux PM brushless DC motor," *J. Asian Electr. Veh.*, vol. 11, no. 2, 1645–1651, 2013. [CrossRef]
2. FNU, and J. Nishanth, "Verdeghem ve E. Severson, A Review of Axial Flux Permanent Magnet Machine Technology", *IEEE Transactions on Industry Applications*,vol. 59, no. 4, pp. 3920 - 3933, 2023.
3. A. S. Çabuk, and Ö. Üstün, ""'Thermal optimization of a radial flux permanent magnet synchronous motor with axial division,"' *Turk J Electr Power Energy Syst*," vol. 3, no. 2, pp. 61–68, 2023.
4. H. Saavedra, L. Romeral, and J. R. Riba, "Optimal design of a three-phase AFPM for in-wheel electrical traction.", IEEE International Electric Vehicle Conference (IEVC), 2014. [CrossRef]
5. S. Sjökvist, and S. Eriksson, "Experimental verification of a simulation model for partial demagnetization of permanent magnets," *IEEE Trans. Magn.*, vol. 50, no. 12, 1–5, 2014. [CrossRef]
6. K. Kim, K. Kim, H. Kim, and J. Lee, "Demagnetization analysis of permanent magnets according to rotor types of interior permanent magnet synchronous motor," *IEEE Trans. Magn.*, vol. 45, no. 6, pp. 2799 - 2802, 2009.
7. X. Wang, Y. Zhang, and N. Li, "Analysis and reduction of electromagnetic noise of yokeless and segmented armature axial flux motor.", 25th International Conference on Electrical Machines and Systems (ICEMS), Chiang Mai, 2022. [CrossRef]
8. X.Wang, X.Zhao, P. Gao, and T. Li, "A new parallel magnetic circuit axial flux permanent magnet in-wheel motor.", 24th International Conference on Electrical Machines and Systems (ICEMS), Gyeongju, 2021. [CrossRef]
9. W.Geng, J. Hou, and Q. Li, "Electromagnetic analysis and efficiency improvement of axial-flux permanent magnet motor with yokeless stator by using grain-oriented silicon steel," *IEEE Trans. Magn.*, vol. 58, no.2, 1–5, 2022. [CrossRef]
10. N.Taran, D. Klink, G.Heins, V. Rallabandi, and D. Patterson, "*A Comparative Study of Yokeless and Segmented Armature versus Single Sided Axial Flux PM Machine Topologies for Electric Traction*," IEEE Energy Conversion Congress and Exposition (ECCE), 2019.
11. J. C. Kappatou, G. D. Zalokostas, and D. A. Spyratos, "Design optimization of axial flux permanent magnet (AFPM) synchronous machine using 3D FEM analysis," *J. Electromagn. Anal. Appl.*, vol. 08, no. 11, 247–260, 2016. [CrossRef]
12. S. S. Soe, and Y. A. Oo, "Design of slotted and slotless AFPM synchronous generators and their performance comparison analysis by using FEA method," *Int. J. Electr.*, vol. 5, no. 4, 2015. [CrossRef]
13. S.Gerçekçioğlu, and M. Akar, "Efficiency and performance comparison between synchronous reluctance and induction motor in axial flux concept," *Fen Bilimleri Derg. Part C Tasarım Teknoloji*, vol. 9, no. 2, pp. 297–316, 2021.
14. N.Pamuk, "Genetik algoritma optimizasyonu kullanılarak senkron makine tasarımı ve uygunluk parametrelerinin belirlenmesi," *Yenilikçi Mühendisli Doğa Bilimleri Derg.*, vol. 4, no. 2, pp. 276 - 288, 2024.
15. F. Marcolini, G. De Donato, F. Giulii Capponi, M. Incurvati, and F. Caricchi, "Design of a multiphase coreless axial flux permanent magnet machine for unmanned aerial vehicle propulsion." 2020 IEEE Energy Conversion Congress and Exposition (ECCE), 2020, 2020. [CrossRef]
16. J. Y. Lee, J. H. Lee, and T. K. Nguyen, "Axial-flux permanent-magnet generator design for hybrid Electric propulsion drone applications," *Energies*, vol. 14, no. 24, 2021. [CrossRef]
17. M. Bonnet, Y. Lefevre, J. F. Llibre, D. Harribey, F. Defay, and N. Sadowski, "3D magnetic field model of a permanent magnet ironless axial flux motor with additively manufactured non-active parts," International Symposium on Electromagnetic Fields in Mechatronics, Electrical and Electronic Engineering (ISEF), 2019. [CrossRef]
18. D. Joshi, D. Deb, and S. M. Muyeen, "Comprehensive review on Electric propulsion system of unmanned aerial vehicles," *Front. Energy Res.*, vol. 10, 2022. [CrossRef]
19. C. Amici, F. Ceresoli, M. Pasetti, M. Saponi, M. Tiboni, and S. Zanoni, "Review of propulsion system design strategies for unmanned aerial vehicles," *Appl. Sci.*, vol. 11, no. 11, 2021. [CrossRef]
20. E.Çetin, and F.Daldaban, "Eksenel akılı motorlarda oluk açıklıklarındaki hatanın moment üzerine etkisi"', El-Cezerî Fen ve Mühendislik," *Dergisi*, vol. 4, no. 3, pp. 374 - 381, 2017.
21. P. Luk, H. Abdulrahem, ve B. Xia, *"Low-cost high-performance ferrite permanent magnet machines in EV applications: A comprehensive review", eTransportation*, Vol. 6, 2020.
22. M. Schiestl *et al.*, "Development of a high power density drive system for unmanned aerial vehicles," *IEEE Trans. Power Electron.*, vol. 36, no. 3, 3159–3171, 2020. [CrossRef]
23. A. Mahmoudi, S. Kahourzade, N. A. Rahim, H. W. Ping, and M. N. Uddin, "Design and prototyping of an optimised axial-flux permanent-magnet synchronous machine," *IET Electr. Power Appl.*, vol. 7, No. 5, 338–349, 2013. [CrossRef]
24. G. Donato, F. Capponi, and F. Carrichi, "On the use of magnetic wedges in axial flux permanent magnet machines," *IEEE Trans. Ind. Electron.*, vol. 60, no. 11, 2013.
25. F. Marignetti, V. Colli, and Y. Coia, "Design of axial flux PM synchronous machines through 3-D coupled electromagnetic thermal and fluid-dynamical finite-element analysis," *IEEE Trans. Ind. Electron.*, vol. 55, no. 10, pp. 3591 - 3601, 2008.
26. S. Huang, J. Luo, F. Leonardi, and T. A. Lipo, "A general approach to sizing and power density equations for comparison of electrical machines," *IEEE Trans. Ind. Appl.*, vol. 34, no. 1, pp. 92 - 97, 1998.
27. S. Huang, J. Luo, F. Leonardi, and T. A. Lipo, "A comparison of power density for axial flux machines based on general purpose sizing equations", *IEEE Trans. Energy Convers.*, vol. 14, no. 2, pp. 185 - 192, 1999.
28. A. Mahmoudi, S. Kahourzade, N. A. Rahim, ve W. P. Hew, "Design, analysis, and prototyping of an axial-flux permanent magnet motor based on genetic algorithm and finite-element analysis," *IEEE Trans. Magn.*, vol. 49, no. 4, 1479–1492, 2013. [CrossRef]
29. M. J. Kamper, W. R. Jie, ve F. G. Rossouw, "Analysis and performance of axial flux permanent-magnet machine with air-cored nonoverlapping concentrated stator windings," *IEEE Trans. Ind. Appl.*, vol. 44, no. 5, pp. 1495 - 1504, 2008.
30. A. S. Çabuk, Ş. Sağlam, ve Ö. Üstün, "Investigation on efficiency of in-wheel BLDC motors for different winding structures," *J. Fac. Eng. Archit. Gazi Univ.*, vol. 34, no. 4, pp. 1975–1985, 2019.